Summer 6-9-2015

Kinetic Study of the Oxygen Reduction Reaction on α-Ni(OH)2 and α-Ni(OH)2 Supported on Graphene Oxide

Elaheh Farjami
CUNY New York City College of Technology

L. Jay Deiner
CUNY New York City College of Technology

Recommended Citation
Farjami, E., & Deiner, L. J. (2015). Kinetic Study of the Oxygen Reduction Reaction on α-Ni (OH) 2 and α-Ni (OH) 2 Supported on Graphene Oxide. Journal of The Electrochemical Society, 162(9), H571-H578.

Kinetic Study of the Oxygen Reduction Reaction on α-$Ni(OH)_2$ and α-$Ni(OH)_2$ Supported on Graphene Oxide

Elaheh Farjami*,z and L. Jay Deiner,z**

Department of Chemistry, NYC College of Technology, City University of New York, Brooklyn, New York 11201, USA

The kinetics of the oxygen reduction reaction on α-$Ni(OH)_2$ and α-$Ni(OH)_2$ supported on graphene oxide (α-$Ni(OH)_2$/GO) were investigated using rotating disk linear sweep voltammetry in alkaline solutions of varying oxygen and hydroxyl concentrations. Over the full hydroxyl concentration range (0.05 M to 0.5M), α-$Ni(OH)_2$/GO displayed higher activity than unsupported α-$Ni(OH)_2$. The electron transfer numbers were 2.9 ± 0.2 for α-$Ni(OH)_2$, 3.4 ± 0.1 for α-$Ni(OH)_2$/GO at low [OH^-], and 3.8–3.9 for α-$Ni(OH)_2$/GO at high [OH^-]. Compared to α-$Ni(OH)_2$, α-$Ni(OH)_2$/GO displayed higher chemical reaction rate constants and higher electron transfer rate constants. These differences suggest that the synergy between the α-$Ni(OH)_2$ catalyst and the graphene oxide support is related to increases in both the speed of the rate determining chemical step and the facility for electron transfer. The order of reaction with respect to oxygen was ∼1 for α-$Ni(OH)_2$ and α-$Ni(OH)_2$/GO. The order of reaction with respect to hydroxyl was ∼0 for α-$Ni(OH)_2$ and α-$Ni(OH)_2$/GO. The first order reaction with respect to oxygen is precedented, but the zero reaction order with respect to hydroxyl is particular to the α-$Ni(OH)_2$ catalysts. The zero reaction order is explained by possible decoupling of solution and catalyst surface hydroxyl concentrations.
 [DOI: 10.1149/2.0041509jes] All rights reserved.

Manuscript submitted April 20, 2015; revised manuscript received May 26, 2015. Published June 9, 2015.

Full utilization of renewable energy resources will require innovation in electrochemical energy conversion and storage technologies including hydrogen-oxygen fuel cells, direct alcohol fuel cells, and metal-air batteries. A common challenge to development of these technologies is the need for electrocatalysis of the oxygen reduction reaction.[1–4] The oxygen reduction reaction is more efficiently catalyzed in alkaline electrolyte,[5] but even in this medium, the performance of the present commercial Pt/C catalysts is non-optimal.[6] The Pt/C catalysts lack durability resulting in unacceptably rapid degradation of activity through time. In addition, the high cost of platinum metal would remain an issue even if catalytic performance were ideal.[7] Thus, a critical materials challenge is the development of low cost, high activity electrode materials to catalyze the oxygen reduction reaction in alkaline media.

Considerable effort has been devoted to the development of oxygen reduction reaction catalysts based on non-platinum transition metals, especially metal oxides and hydroxides. In these works, oxides (or hydroxides) of manganese and cobalt have received the majority of the attention with particularly promising results demonstrated for CoO/carbon nanotube hybrids, carbon-supported MnO_x/C, and a Co_3O_4/N-doped graphene hybrid.[8–11] In contrast to manganese and cobalt, comparatively little work has been directed toward evaluating the different phases of nickel oxide or hydroxide as catalysts for the oxygen reduction reaction. Such work may uncover new oxygen reduction reaction catalysts, and may also clarify the mechanism by which doping with nickel hydroxide enhances activity and durability of MnO_x catalysts.[10,12]

Recently, a simple one-step microwave synthesis of alpha nickel hydroxide supported on graphene oxide (α-$Ni(OH)_2$/GO) has been developed.[13] The synthesized α-$Ni(OH)_2$/GO catalyst revealed promising activity toward the oxygen reduction reaction in alkaline media. This is in contrast to the relatively poor performance of β-$Ni(OH)_2$ which exhibits low activity for the oxygen reduction reaction, attributed to the difficulty of low temperature formation of NiOOH from $Ni(OH)_2$.[14] The activity of the α-$Ni(OH)_2$/GO catalyst was greater than the unsupported α-$Ni(OH)_2$ catalyst, and greater than the graphene oxide (GO) support alone. Specifically, the onset potential of the oxygen reduction reaction on the α-$Ni(OH)_2$/GO catalyst was lower than the onset potential of the reaction on either the support or the α-$Ni(OH)_2$ particles alone. Similarly, the peak current density on the hybrid catalyst was higher than the corresponding current density on either the unsupported α-$Ni(OH)_2$ particles or the support alone.[13] This suggests a synergistic interaction between alpha nickel hydroxide particles and the graphene oxide support, a phenomenon previously observed for Co_3O_4 supported on graphene.[9] Preliminary rotating disk electrode (RDE) studies provided evidence that the oxygen reduction reaction on α-$Ni(OH)_2$/GO proceeded primarily through a 4e^- pathway in alkaline solution.[13]

While the observed activity of the α-$Ni(OH)_2$/GO catalyst was encouraging, fundamental kinetic questions remained regarding the oxygen reduction reaction on this material. The first question was whether the reaction mechanism on the α-$Ni(OH)_2$/GO catalyst was distinct from that on the unsupported α-$Ni(OH)_2$ catalyst. Comparison of the mechanisms would provide insight into the origin of the synergy between the α-$Ni(OH)_2$ catalyst and the graphene oxide support. The second question was how the reaction mechanisms on the supported and unsupported α-$Ni(OH)_2$ catalysts compared to established mechanisms for other transition metals, especially oxides and hydroxides of manganese and cobalt.

In alkaline solution, the oxygen reduction reaction can follow a direct four electron pathway, a two electron pathway, or a sequential four electron pathway.[15] These pathways are each comprised of multiple elementary steps, but the overall pathways may be summarized by three reactions. The direct 4e^- pathway entails conversion of O_2 to OH^- (Equation 1).

$$O_2 + 2H_2O + 4e^- \rightarrow 4OH^- \quad [1]$$

The 2e^- pathway converts O_2 to HO_2^- (Equation 2).

$$O_2 + H_2O + 2e^- \rightarrow HO_2^- + OH^- \quad [2]$$

The HO_2^- may either desorb from the catalyst surface, or it may persist enabling a further 2e^- reduction to OH^- (Equation 3). This second step completes the 4e^- transfer of the sequential mechanism.

$$HO_2^- + H_2O + 2e^- \rightarrow 3OH^- \quad [3]$$

For electrocatalytic devices, a four electron transfer, whether through a direct or sequential pathway, is preferable. The electron transfer numbers reported for carbon support materials such as carbon black and the pristine reduced graphene oxide (RGO) are about 2.5 and 2.7, respectively.[10,16] For the MnO_x/C and RGO–MnO_2 the electron transfer numbers for the oxygen reduction reaction increase to 3.54 and 3.8, values similar to those for commercially available Pt/XC-72.[10,16] Depending on the nanostructures and shapes of MnO_2, reported electron transfer numbers for MnO_2 vary from 2.9 to 3.9.[17] For N-doped graphene supported Co_3O_4, the electron transfer number is 3.9, and for transition metal hydroxides such β-$Co(OH)_2$/C and β-$Ni(OH)_2$/C

*Electrochemical Society Student Member.
**Electrochemical Society Active Member.
zE-mail: farjami.elahe@gmail.com; Ldeiner@citytech.cuny.edu

the number of electrons transferred in the oxygen reduction reaction are close to 3 and 4, respectively.[9,11,14] However, as stated above, the activity of the β-$Ni(OH)_2$ catalyst is quite low. The order of reaction with respect to O_2 is ∼1 for MnO_x and CoO_x,[9–10] similar to that reported for precious metal catalysts.[18–20] The order of reaction with respect to hydroxyl is −0.5 for MnO_x.[10]

In this study, we use rotating disk electrode linear sweep voltammetry to evaluate the kinetics of the oxygen reduction reaction on microwave synthesized α-$Ni(OH)_2$ and α-$Ni(OH)_2$/GO at a range of hydroxyl and oxygen concentrations. These data enable extraction of electron transfer numbers, reaction orders with respect to oxygen and hydroxyl, and kinetic rate constants. This detailed kinetic information allows for a more complete comparison between the mechanism of the oxygen reduction reaction on supported and unsupported α-$Ni(OH)_2$ and other transition metal oxides and hydroxides. To our knowledge, there is no report that shows the effect of hydroxyl ion concentration and oxygen concentration on the catalytic activity of nickel hydroxide catalysts for oxygen reduction in alkaline solution.

Experimental

Synthesis and characterization.— The $Ni(OH)_2$/GO hybrid catalyst was synthesized based on the procedure described in previous work.[13] Briefly, 50 mg of graphite oxide was dispersed in 100 mL of water, and exfoliation of graphite was achieved by sonication of the dispersion for 2 h in an ultrasonic bath (Fisher Scientific, FS30). After sonication, a brownish dispersion was obtained indicating exfoliation of the graphite to produce graphene oxide. After exfoliation, 1.64 g of nickel (II) acetate (Acros Organics, 99+%) and 6.77 g of urea (Acros Organics, 99.5%) were added to the graphene oxide dispersion while stirring for 30 min. This procedure was followed by microwave (General Electric, JES1142SJ) irradiation of the as prepared dispersion. The microwave process was carried out in ambient conditions at a power level of approximately 700 W for 7 min. The resulting black precipitate was collected by filtration, washed three times with distilled water, and dried at 100°C for 12 h in a vacuum oven. Pure $Ni(OH)_2$ nanostructures were synthesized by the same procedure as described above, but in the absence of graphene oxide.

Characterization of the $Ni(OH)_2$ nanoparticles and the $Ni(OH)_2$/GO hybrid catalyst was performed by X-ray diffraction (XRD), scanning electron microscopy (SEM), and diffuse reflectance infrared Fourier transform spectroscopy (DRIFTS).[13] X-ray diffraction measurements showed a rhombohedral α-$Ni(OH)_2$ crystalline structure in both the presence and absence of the graphene oxide support. SEM images revealed a homogeneous distribution of supported $Ni(OH)_2$ nanoparticles (∼150–200 nm, rhombohedral particles and platelets) with no undecorated graphene oxide sheets. Distinct rhombus-shaped particles in the range of 250–300 nm were observed for the unsupported $Ni(OH)_2$. Diffuse reflectance infrared spectroscopy showed the disappearance of the C=O bonds on the graphene oxide sheet after the synthesis with $Ni(OH)_2$. This suggested that the graphene oxide sheet was reduced.

Electrochemical measurements.— Linear sweep voltammetry measurements were carried out with a potentiostat/galvanostat/FRA (Princeton Applied Research, PARSTAT 2273) in a conventional one-compartment glass three-electrode cell (Princeton Applied Research, Analytical Cell Kit, Model RDE 0018). A glassy carbon disk (Princeton Applied Research, 5 mm diameter) was used as support for the catalysts and served as the working electrodes during the electrochemical measurements. Electrode rotation was accomplished with a manually set electrode rotator (Princeton Applied Research, Model 636). A Pt wire coil (BASi) was used as the counter electrode, and the reference electrode was Ag/AgCl (CH Instruments, 1 M KCl). This reference electrode potential is +234 mV versus NHE.[21–22] Linear sweep voltammetry (LSV) rotating disk electrode (RDE) measurements were carried out at a rate of 5 mV s^{-1} from 0.05 V to −0.7 V vs. Ag/AgCl. Rotational speeds were varied from 100 to 2000 rpm. Prior to use, the glassy carbon disk electrode was polished with 1.0, 0.3 and 0.05 μm alumina powder, and then cleaned via sonication in an ethanol-water bath for ∼3 min. The electrode was then sonicated in 18 MΩ water for ∼3 min. To prepare the catalyst inks for the electrode modification, 1 mg of catalyst was dispersed in 1 mL of N,N-dimethylformamide (DMF), and sonicated with a sonic wand (Sonics, Vibra Cell), for 60 min to form a homogenous ink. This ink was then re-sonicated for 60 min in a bath sonicator immediately prior to functionalization of the working electrode. After dispersion, 9.0 μL of catalyst ink was loaded onto the 5 mm glassy carbon electrode which was dried in an oven for a minimum of two hours to evaporate the solvent. For the electrochemical measurements, aqueous solutions of NaOH (Fluka, Analytical Grade) at the desired concentrations were prepared in 18 MΩ water (Milli-Q) and used as the supporting electrolyte. The solutions were purged with argon for 20 minutes for O_2-free scans. The argon purge was removed from the solution during scanning, but flow was continued in the free area in the cell above the electrolyte. For O_2-saturated scans, O_2 was bubbled into the supporting electrolyte for 20 min. The oxygen purge was removed from the solution during scanning, but flow was continued in the free area in the cell above the electrolyte. Ambient oxygen concentration was achieved without any bubbling.

Results and Discussion

Figure 1 shows constant rotation rate linear sweep voltammograms of the α-$Ni(OH)_2$ and α-$Ni(OH)_2$/GO recorded for hydroxyl concentrations of 0.05 M, 0.1 M, and 0.5 M, and oxygen partial pressures of saturation (1 atm) and ambient (0.2 atm). The linear sweep voltammograms recorded in an oxygen-free, Ar-saturated NaOH solution are featureless in this potential window (data not shown) confirming that the α-$Ni(OH)_2$ and α-$Ni(OH)_2$/GO hybrid are electro-inactive in the absence of oxygen in this region. Irrespective of the oxygen or hydroxyl concentration, a more positive onset potential and higher peak current is observed for the α-$Ni(OH)_2$/GO as compared to the α-$Ni(OH)_2$ alone. The onset potentials for both the α-$Ni(OH)_2$ and α-$Ni(OH)_2$/GO catalyst are also lower and the peak current higher as compared to the graphene oxide support alone.[13] The observation that the α-$Ni(OH)_2$/GO catalyst has lower onset potential and higher current than either the graphene oxide support or α-$Ni(OH)_2$ alone suggest that the catalyst and support act in synergy. This phenomenon has been documented previously for 0.5 M NaOH concentration,[13] and is now confirmed for the present less alkaline conditions of 0.05 M and 0.1 M.

The unsupported catalyst at the lowest hydroxyl concentration (0.05 M) shows a slightly inclined current between −0.45 V and −0.55 V, and then displays an increasingly sloped current at potentials beyond −0.55 V. The observation of a sloped plateau region in rotating disk electrode measurements is common in studies of electrocatalytic reactions, especially the oxygen reduction reaction.[23–26] Based on a simple kinetic model of a two-step process involving chemical interaction with the catalyst followed by an electron transfer step, it can be shown that the inclined plateau regions arise from the presence of a range of active sites with different reduction potentials and from the relative rates of the chemical step versus the electron transfer step.[23] In contrast, the shape of the linear sweep voltammograms of the supported α-$Ni(OH)_2$ catalyst does not display significant slope, even at high overpotential and low hydroxyl concentration; for all hydroxyl concentrations from 0.05 M to 0.5 M, the oxygen reduction reaction on α-$Ni(OH)_2$/GO shows a flat limiting current region between −0.4V and −0.6V.

Electron transfer number of the oxygen reduction reaction.— Rotating disk electrode measurements were performed at different working electrode rotation rates in order to determine the electron transfer numbers for the oxygen reduction reaction on the supported and unsupported $Ni(OH)_2$ as a function of hydroxyl concentration. The electron transfer numbers were calculated using the slopes of the Levich plots[27–28] (Figure 2) in which the inverse of the Levich or limiting current was plotted against the inverse square root of the rotation rate,

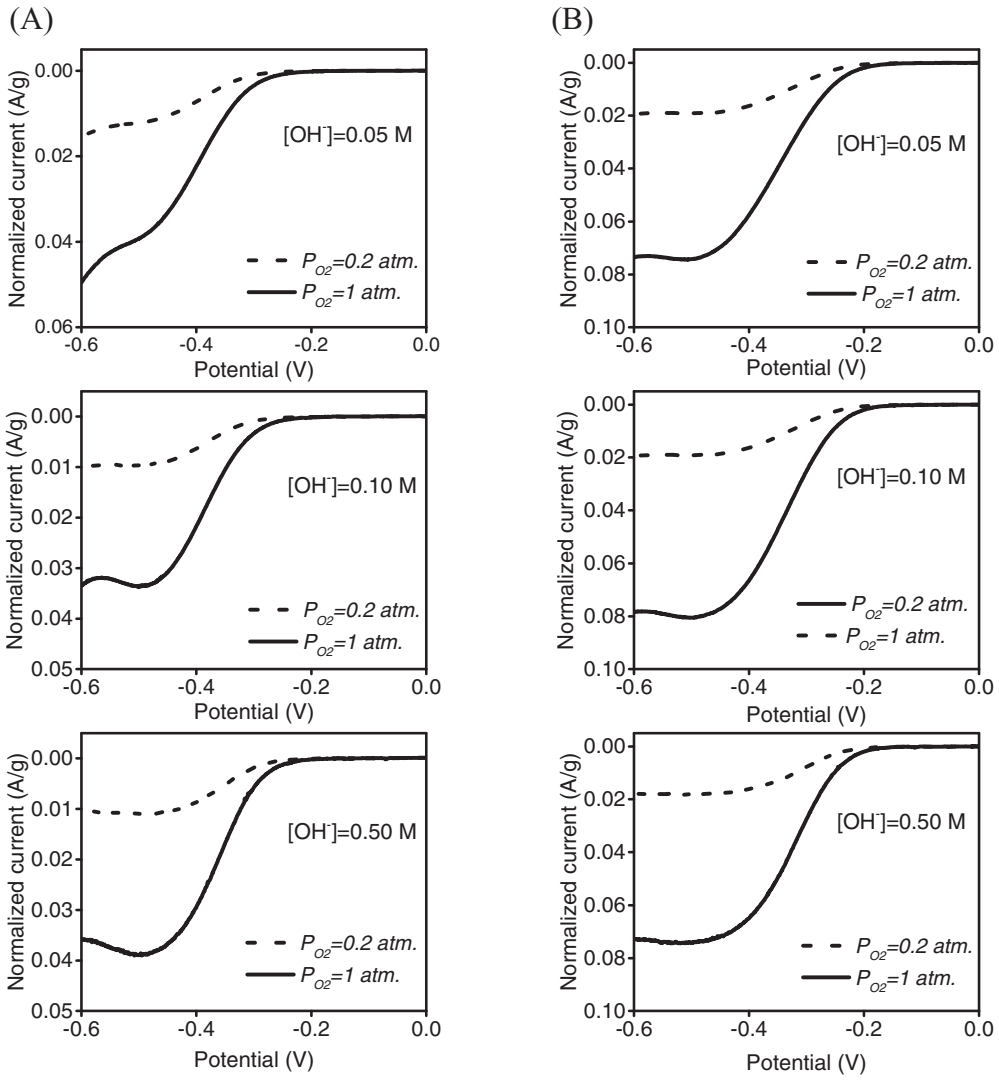

Figure 1. Linear sweep voltammograms for catalytic oxygen reduction reaction at (A) α-$Ni(OH)_2$, and (B) α-$Ni(OH)_2$/GO in O_2-saturated and ambient O_2 concentrations, and at NaOH solutions at concentrations of 0.05 M, 0.1 M, and 0.5 M. Rotation rate: 2000 rpm, T = 25°C. Current has been normalized using the total mass of catalyst material deposited.

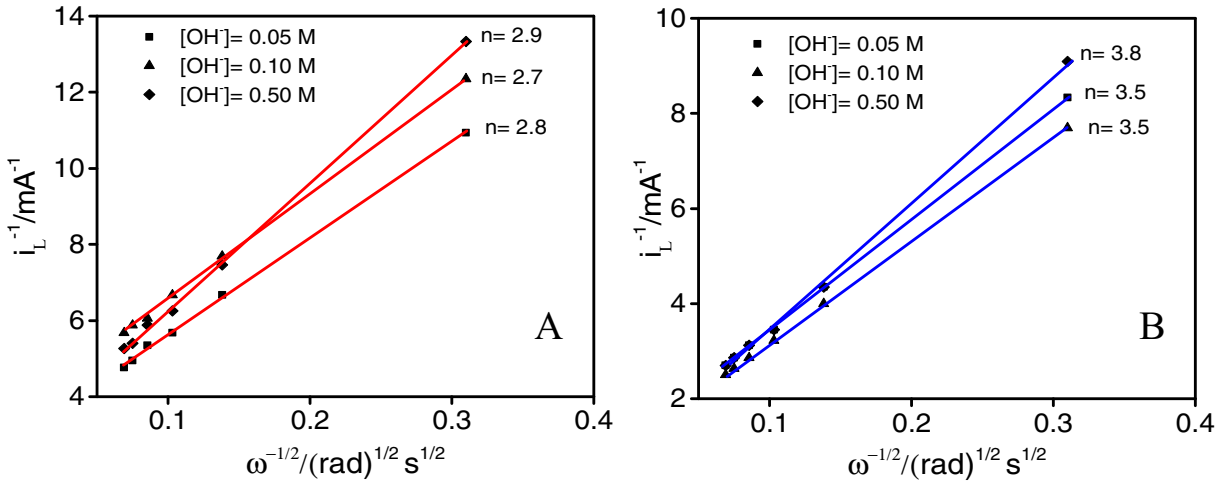

Figure 2. Levich plots for the limiting O_2 reduction current at (A) α-$Ni(OH)_2$, and (B) α-$Ni(OH)_2$/GO electrodes (i_L measured at E = −0.45 V vs. Ag/AgCl) in NaOH solutions saturated with O_2.

Table I. Values of the NaOH concentration dependent solution oxygen concentrations (C_{O2}), viscosities and diffusion coefficients.[38]

C_{NaOH}/M	C_{O2}/mol cm^{-3}	Viscosity/ mPa · s	Diffusion Coefficients D_{O2}, cm^2/s
0.05	6.0×10^{-7}	0.9017	1.73×10^{-5}
0.10	5.8×10^{-7}	0.9032	1.73×10^{-5}
0.50	4.5×10^{-7}	0.9145	1.70×10^{-5}

as described in Equation 4:

$$i_L = 0.62nFAC_{O_2}\omega^{1/2}{D_{O_2}}^{2/3}v^{-1/6} \quad [4]$$

Here, i_L is Levich or limiting current (generally stable in the range of −0.40 V to −0.55 V in this work), ω is the rotation rate, F is the Faraday constant, C_{O2} is the saturation concentration of oxygen, D_{O2} is the diffusion coefficient of O_2 in the NaOH solution, and v is the kinematic viscosity of the solution. Since the saturation oxygen concentration, solution viscosity, and oxygen diffusion coefficient vary as a function of inorganic electrolyte concentration,[29–30] the values of C_{O2}, v, and D_{O2} were calculated for NaOH concentrations of 0.05 M, 0.1 M, and 0.5 M, and are summarized in Table I.[31] Based on the NaOH concentration corrected values listed in Table I, n, the electron transfer number, was readily calculated from the Levich slopes ($0.62nFC_{O_2}{D_{O_2}}^{2/3}v^{-1/6}$) (representative Levich plot for the current measured at −0.45 V is shown in Figure 2). The electron transfer numbers for overpotentials between −0.40 V and −0.55 V are summarized in Table II. The electron transfer numbers for the unsupported α-$Ni(OH)_2$ fall in the range of 2.9 ± 0.2, consistent across the range of hydroxyl concentrations. For the α-$Ni(OH)_2$/GO hybrid catalyst, the electron transfer numbers for the oxygen reduction reaction in 0.05 M NaOH and 0.1M NaOH are in the range of 3.4 ± 0.1. In 0.5 M NaOH, the electron transfer numbers range from 3.8 to 3.9.

The observation that the electron transfer numbers are neither exactly two nor exactly four suggests that for α-$Ni(OH)_2$ and α-$Ni(OH)_2$/GO, the measured current is likely due to simultaneous reduction of oxygen through four electron and two electron pathways. The observation that the α-$Ni(OH)_2$/GO catalyst displays higher electron transfer numbers than the free α-$Ni(OH)_2$ catalyst indicates that, although both catalysts permit simultaneous two and four electron mechanisms, the four electron pathway is more favorable on the α-$Ni(OH)_2$/GO hybrid catalyst as compared to the unsupported α-$Ni(OH)_2$ catalyst. In fact, while the electron transfer numbers calculated for the unsupported α-$Ni(OH)_2$ catalyst suggest a quite significant proportion of two electron transfer, the electron transfer numbers calculated for the supported catalyst suggest predominant four electron transfer. For unsupported α-$Ni(OH)_2$, the proportion of two and four electron transfer pathways does not vary significantly with hydroxyl concentration for the range of potentials in which Levich current is stable. For α-$Ni(OH)_2$/GO, the proportion of four electron transfer increases slightly at the highest hydroxyl concentration of 0.5 M.

Table II. Summary of electron transfer numbers for catalytic oxygen reduction reaction at $Ni(OH)_2$ and $Ni(OH)_2$/GO catalysts in O_2-saturated solution with [OH^-] of 0.05 M, 0.1M, and 0.5M.

Potential	Electron transfer number/n					
	[OH^-]/M			[OH^-]/M		
E (V)	0.05	0.10	0.50	0.05	0.10	0.50
−0.40	3.0	3.1	2.9	3.4	3.5	3.9
−0.45	2.8	2.7	2.9	3.5	3.5	3.8
−0.50	3.1	2.7	2.9	3.3	3.5	3.9
−0.55	3.1	2.7	2.8	3.3	3.3	3.8

Kinetic rate constants.— In addition to providing the electron transfer numbers, the linear sweep rotating disk electrode measurements furnished pH-dependent kinetic rate constants for oxygen reduction on α-$Ni(OH)_2$/GO and unsupported α-$Ni(OH)_2$.[32] In order to obtain these values, Koutecky-Levich plots were created in which the inverse of the total measured current is plotted against the inverse square root of the rotation rate (Figure 3). For these plots, the total measured current is interpreted as a function of the Levich (limiting) and kinetic currents, Equation 5, where i_L (A) is the Levich current, and i_k (A) is the kinetic current.

$$i^{-1} = {i_K}^{-1} + {i_L}^{-1} \quad [5]$$

These currents, in turn, can be expressed in terms of the electron transfer numbers, the kinetic rate constant, and physical parameters of the experiment, Equation 6.

$$i^{-1} = 1/(nFAK\Gamma_{cat}C_{O_2}) + 1/0.62nFAC_{O_2}\omega^{1/2}{D_{O_2}}^{2/3}v^{-1/6} \quad [6]$$

K ($cm^3mol^{-1}s^{-1}$) is the kinetic rate constant for a catalytic reaction, F (A · s/mol) is the Faraday constant, A (cm^2) is the electrode area, Γ_{cat} (mol/cm^2) is the areal concentration of catalyst on the surface of the electrode, C_{O2} (mol/cm^3) is the solution concentration of oxygen, n is the electron transfer number per mole of a reactive species, ω (s^{-1}) is the rotation rate obtained by converting rotations per minute to radians per second, D_{O2} (cm^2. s^{-1}) is the diffusion coefficient of the oxygen, and v (cm^2. s^{-1}) is the viscosity of the solution. From the comparison of Equations 5 and 6, it is clear that the intercepts of Koutecky-Levich plots ($\omega^{-1/2} = 0$), can be used to determine the kinetic current. Using this intercept and the NaOH concentration-dependent values of C_{O2}, D_{O2}, and v (Table I), and the calculated electron transfer numbers (from the slope of the Koutecky-Levich plots) the kinetic rate constant, K, was determined as a function of applied potential for each hydroxyl concentration (Table III). As can be seen from the ratios of the kinetic rate constants on the two catalysts, irrespective of the potential, the kinetic rate constant is always larger for the α-$Ni(OH)_2$/GO hybrid catalysts as compared to the unsupported α-$Ni(OH)_2$. The larger kinetic rate constant observed for the α-$Ni(OH)_2$/GO hybrid supports the interpretation that the synergy between the α-$Ni(OH)_2$ and the graphene oxide leads to a greater activity for the oxygen reduction reaction on the hybrid catalyst. This synergistic action is evident throughout the whole range of hydroxyl concentrations studied. In fact, the ratio of the α-$Ni(OH)_2$/GO kinetic rate constant to the α-$Ni(OH)_2$ kinetic rate constant increases with increasing hydroxyl concentration.

More detailed examination of the potential dependence of the kinetic rate constant enables deconvolution of the constant into chemical reaction rate constants and electron transfer rate constants.[33] As the kinetic rate constant contains contributions from the rates of purely chemical processes and from the rates of electron transfer processes, the kinetic rate constant can be described as follows (Equation 7):[33]

$$1/K = 1/K_c + 1/K_e\exp(-(\alpha n_\alpha F/RT)(E-E^0)) \quad [7]$$

K_c is the chemical reaction rate constant, K_e is the electron transfer rate constant, α is the electron transfer coefficient in the rate determining step, n_α is the electron transfer number in the rate determining step, E is the applied potential, and E^0 is the thermodynamic potential. F, R, and T are the Faraday constant, the ideal gas constant, and the temperature, respectively. For the oxygen reduction reaction, K_c is typically interpreted to correspond to the rate constant for the adsorption of O_2 on the catalyst active site, and K_e is the electron transfer rate constant for the rate determining electron transfer step. For this electron transfer step, the corresponding electron transfer number, n_α, is typically accepted as 1.[33] Based on Equation 7, it is clear that at high overpotentials, the electron transfer contribution to the total kinetic rate constant approaches 0, and the kinetic rate constant becomes potential independent and equal to the chemical reaction rate constant. In Table III, the kinetic rate constants increase from −0.28 V to ∼ −0.45 V. For potentials beyond −0.45 V, the kinetic rate constant approximates potential independence. The averages of the kinetic rate constants in this potential independent region approximate the value

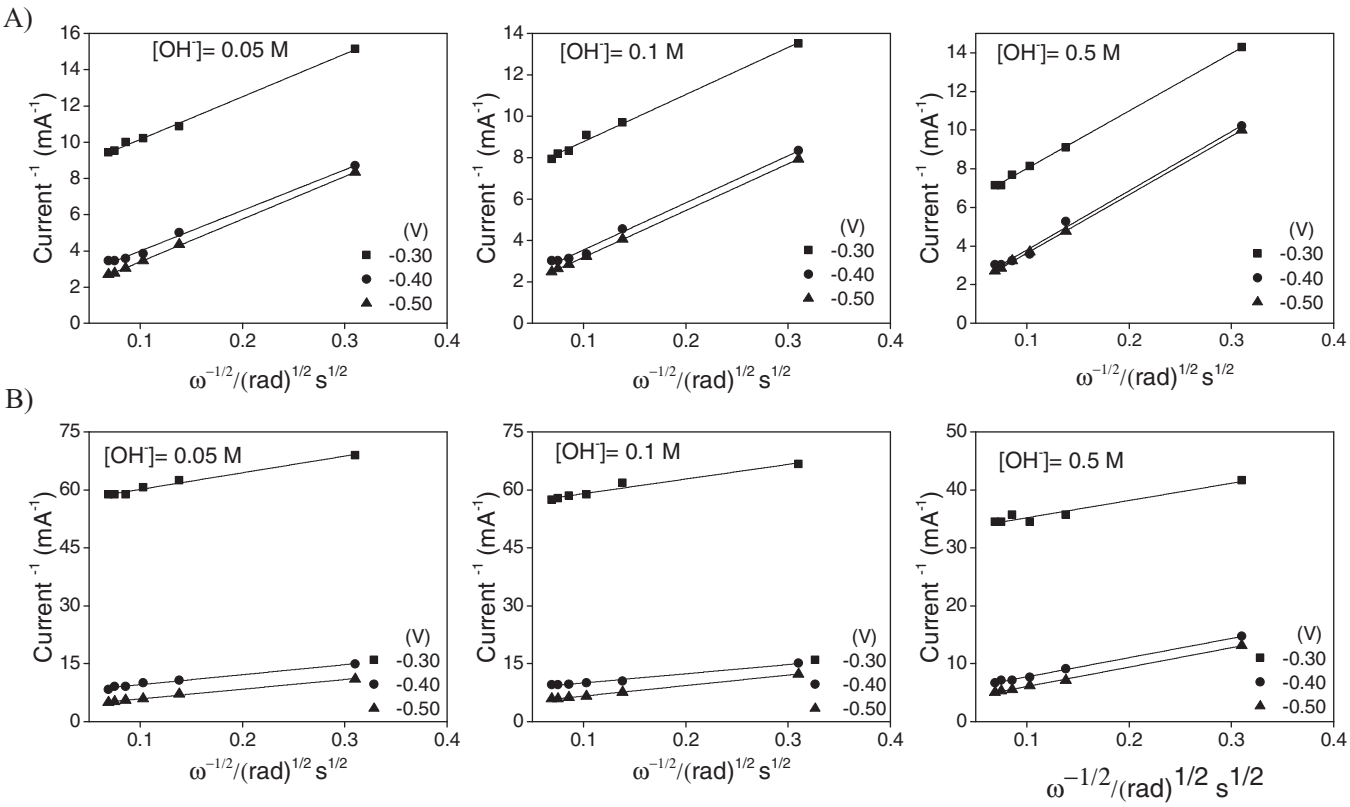

Figure 3. Koutecky-Levich plots for the oxygen reduction reaction at (A) α-Ni(OH)$_2$/GO, and (B) α-Ni(OH)$_2$ catalysts in O$_2$-saturated solution of NaOH at the labeled concentrations.

of the chemical reaction rate constants, K_c. These values are summarized in Table IV for α-Ni(OH)$_2$ and α-Ni(OH)$_2$/GO for all of the measured hydroxyl concentrations. For hydroxyl concentrations of 0.05 M and 0.1 M, the value of K_c for α-Ni(OH)$_2$/GO is 2–3 times as high as the corresponding value on α-Ni(OH)$_2$. For the hydroxyl concentration of 0.5M, the value of K_c is nearly ten times higher on the supported catalyst. The differences between K_c on the supported and unsupported catalyst suggest that part of the synergy between the α-Ni(OH)$_2$ catalyst and the graphene oxide support can be traced to an increased rate constant for O$_2$ adsorption on the supported catalyst. By simple Arrhenius kinetics, this would imply that the activation energy for adsorption on the supported catalyst may be lower as compared to the unsupported catalyst. The hypothesized lower activation energy for O$_2$ adsorption on the supported catalyst would contribute to the synergistic affect observed between the α-Ni(OH)$_2$ catalyst and the graphene oxide support.

Using the values of the chemical reaction rate constant, K_c, derived from the potential independent region of the kinetic rate constant, K, it is possible to approximate the electron transfer rate constant, K_e.[33] Specifically, if the value of K_c is substituted into Equation 7, then the logarithm of the equation becomes (Equation 8):

$$\log(1/K - 1/K_c) = \log(1/K_e) + 2.303(\alpha n_\alpha F/RT)(E - E^0) \quad [8]$$

E^0, the thermodynamic potential for the oxygen reduction reaction under the conditions of the present study, is obtained from the Nernst equation (Equation 9) as applied to the oxygen reduction reaction,

Table III. Summary of kinetic rate constants for catalytic oxygen reduction reaction at α-Ni(OH)$_2$ and α-Ni(OH)$_2$/GO hybrid catalysts in O$_2$-saturated solution of NaOH at different concentrations. The final column shows the ratio of the kinetic rate constants for the supported and unsupported catalysts. Kinetic rate constants are calculated based on the electron transfer numbers corresponding to each potential.

Potential	$K\Gamma_{cat\ [Ni(OH)2]}$ /cm s^{-1}			$K\Gamma_{cat\ [Ni(OH)2/GO]}$ /cm s^{-1}			$K\Gamma_{cat\ [Ni(OH)2/GO]}/K\Gamma_{cat\ [Ni(OH)2]}$		
	[OH$^-$]/M			[OH$^-$]/M			[OH$^-$]/M		
E (V)	0.05	0.10	0.50	0.05	0.10	0.50	0.05	0.10	0.50
−0.28	1.4×10^{-3}	1.0×10^{-3}	1.2×10^{-3}	3.6×10^{-3}	5.2×10^{-3}	1.4×10^{-2}	2.6	5.2	11.7
−0.30	1.5×10^{-3}	1.4×10^{-3}	2.4×10^{-3}	5.8×10^{-3}	6.8×10^{-3}	1.5×10^{-2}	3.9	5.0	6.3
−0.32	1.4×10^{-3}	1.7×10^{-3}	3.3×10^{-3}	7.6×10^{-3}	9.3×10^{-3}	2.4×10^{-2}	5.5	5.5	7.2
−0.35	2.9×10^{-3}	2.7×10^{-3}	8.6×10^{-3}	1.2×10^{-2}	1.5×10^{-2}	3.9×10^{-2}	4.0	5.7	4.5
−0.38	2.1×10^{-3}	5.1×10^{-3}	1.1×10^{-2}	1.8×10^{-2}	2.2×10^{-2}	7.7×10^{-2}	8.6	4.3	7.0
−0.40	7.0×10^{-3}	6.1×10^{-3}	1.9×10^{-2}	2.4×10^{-2}	3.5×10^{-2}	1.1×10^{-1}	3.4	5.7	5.6
−0.45	1.5×10^{-2}	1.2×10^{-2}	2.9×10^{-2}	3.2×10^{-2}	5.1×10^{-2}	2.0×10^{-1}	2.1	4.3	6.9
−0.50	1.4×10^{-2}	1.3×10^{-2}	3.1×10^{-2}	4.3×10^{-2}	4.8×10^{-2}	1.3×10^{-1}	3.1	3.7	4.1
−0.55	1.6×10^{-2}	1.3×10^{-2}	2.3×10^{-2}	4.0×10^{-2}	5.7×10^{-2}	2.5×10^{-1}	2.5	4.4	10.8
−0.60	1.5×10^{-2}	1.3×10^{-2}	2.2×10^{-2}	3.1×10^{-2}	3.7×10^{-2}	2.0×10^{-1}	2.1	2.9	9.1

Table IV. Summary of the chemical reaction rate constants (K_c) and the electron transfer rate constants (K_e) for the catalytic oxygen reduction reaction at the α-Ni(OH)$_2$ and α-Ni(OH)$_2$/GO catalysts at hydroxyl concentrations of 0.05 M, 0.1 M, and 0.5 M.

	Ni(OH)$_2$		Ni(OH)$_2$/GO	
[OH$^-$]/M	K_c/cm s^{-1}	K_e/cm s^{-1}	K_c/cm s^{-1}	K_e/cm s^{-1}
0.05	1.5×10^{-2}	2.5×10^{-8}	3.7×10^{-2}	8.5×10^{-8}
0.10	1.3×10^{-2}	9.8×10^{-8}	4.8×10^{-2}	2.2×10^{-7}
0.50	2.6×10^{-2}	2.9×10^{-9}	2.0×10^{-1}	5.6×10^{-7}

described in Equation 1.

$$E^0 = E^{0\prime} + (2.303RT/nF)\log([O_2]/[OH^-]^4) \quad [9]$$

The value of $E^{0'}$, the standard thermodynamic potential, is 0.401 V vs. NHE.[22,34] The values for [O_2], the concentration of oxygen, are as defined in Table I. With the appropriate E^0 values calculated, the intercept of the plots of log (1/K – K_c) versus E-E^0 (Figure 4) can be used to compute the value of K_e, the electron transfer rate constant (Table IV). We note here that application of this treatment to the present catalysts will yield approximate electron transfer rate constants because the above calculation of E^0 is based on a Nernst equation that assumes four electron transfer (based on Equation 1). The actual electron transfer numbers on the supported and unsupported α-Ni(OH)$_2$ catalysts (Table II) suggest contribution of both two and four electron pathways.

For all hydroxyl concentrations in this study, the value of the electron transfer rate constant is greater on the α-Ni(OH)$_2$/GO catalyst as opposed to the unsupported catalyst. Interestingly, the value of the electron transfer rate constant increases steadily on the α-Ni(OH)$_2$/GO catalyst such that for hydroxyl concentrations of 0.5 M, it is more than two orders of magnitude higher than the corresponding electron transfer rate constant on the unsupported α-Ni(OH)$_2$. This suggests that increases in the electron transfer rate may also contribute to the synergy between the α-Ni(OH)$_2$ catalyst and the support.

Reaction orders with respect to O_2 and OH^-.— The influence of oxygen concentration on the oxygen reduction reaction kinetics was investigated to determine the reaction orders with respect to O_2. In order to study the reaction order with respect to oxygen concentration, rotating disk results were obtained for unsupported α-Ni(OH)$_2$ and α-Ni(OH)$_2$/GO catalysts at two different oxygen partial pressures (air: 0.2 atm., and pure oxygen: 1 atm.) at each hydroxyl concentration (data shown in Figure 1). The rate of reaction is reflected in the kinetic current (Equation 10):

$$i_k = k[O_2]^r[OH^-]^m \quad [10]$$

Table V. Summary of reaction orders with respect to P_{O2} for α-Ni(OH)$_2$ alone, and α-Ni(OH)$_2$/GO catalysts.

Catalyst	[OH$^-$] = 0.05 M	[OH$^-$] = 0.10 M	[OH$^-$] = 0.50 M
Ni(OH)$_2$	0.8	0.8	0.7
Ni(OH)$_2$/GO	0.8	0.9	0.9

From the RDE results, the kinetic current densities, i_k, at low overpotentials were tabulated after correction for O_2 diffusion in solution ($i_k = \frac{i_L * i}{i_L - i}$).[35] For constant hydroxyl concentration, the ratio of the low overpotential kinetic currents, $i_{k,1atm}/i_{k,0.2atm}$, then provided the order of reaction with respect to oxygen. Table V represents the reaction orders with respect to oxygen concentration for unsupported α-Ni(OH)$_2$ and α-Ni(OH)$_2$/GO catalysts at different hydroxyl concentrations. The reaction orders are all in the range of 0.8 ± 0.1. These values are close to 1, in agreement with previous reports for MnO_x/C, platinum, and silver.[10,18–20]

The effect of pH on the kinetics of the oxygen reduction reaction was examined to determine the orders of reaction with respect to hydroxyl. To do so, linear sweep voltammograms were obtained at a rotation rate of 2000 rpm with saturated O_2 concentration and varying hydroxyl concentrations. The overpotential of the working electrode at constant current density was recorded to create plots of the polarization voltage as a function of the log of the current density (Figures 5a and 5b).[36] The voltage necessary to sustain low (0.13 mA/cm^2) and high (1.3 mA/cm^2) current densities was then plotted as a function of pH (Figures 5c and 5d). For the α-Ni(OH)$_2$/GO catalyst, at low and high current densities, the slope of the E vs. pH line is quite close to 0 suggesting that the order of reaction with respect to hydroxyl is approximately zero. For the unsupported α-Ni(OH)$_2$, the slope of the line is ∼0.1, suggesting that the order of reaction with respect to hydroxyl may be slightly positive, but also quite close to 0.

The nearly equal orders of reaction with respect to oxygen and hydroxyl on α-Ni(OH)$_2$ and α-Ni(OH)$_2$/GO suggests that the mechanism of reaction on the supported and unsupported catalysts may be similar. Further consideration of the orders of reaction allows comparison of the oxygen reduction reaction mechanism on the current Ni-based catalysts to other transition metal catalysts. Notably, the reaction order with respect to oxygen observed for supported and unsupported α-Ni(OH)$_2$ is close to 1, the same as the reaction order with respect to oxygen for carbon supported MnO_x nanoparticles,[10] and for platinum and silver.[18–20] The first order kinetics with respect to oxygen has been interpreted to indicate that the adsorption of oxygen is a rate determining step in the mechanism.[10] Even though α-Ni(OH)$_2$ and α-Ni(OH)$_2$/GO have the same orders of reaction with respect to oxygen, the higher activity of the supported α-Ni(OH)$_2$ catalyst may be explained by the observation that the chemical reaction rate constant is more rapid on the supported versus unsupported catalyst.

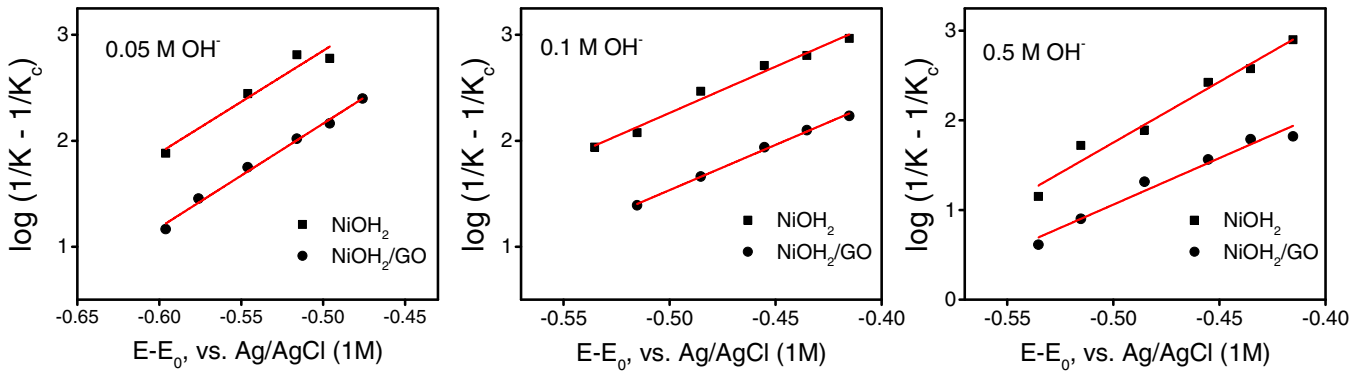

Figure 4. Oxygen reduction reaction kinetic constants as a function of applied electrode potential (E−E_0) at α-Ni(OH)$_2$, and α-Ni(OH)$_2$/GO at three different NaOH concentrations.

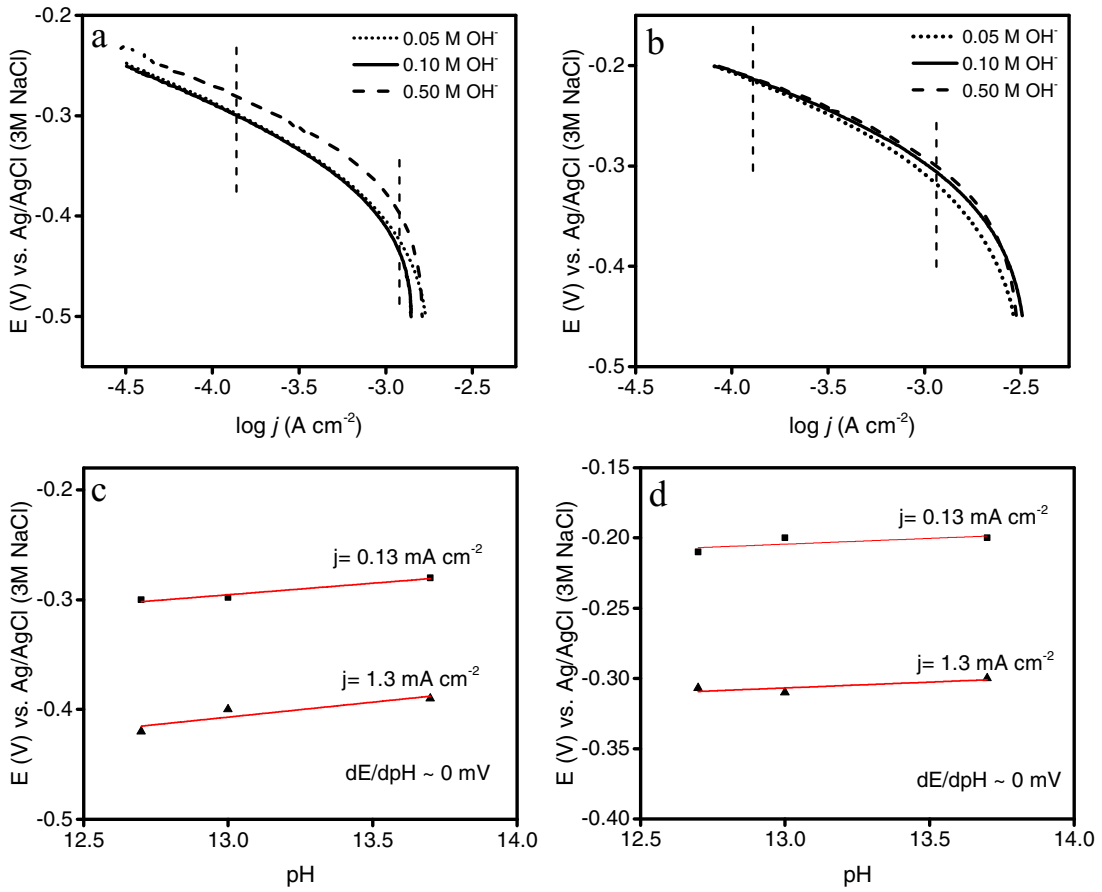

Figure 5. E-log j relationships in alkaline solution of different pHs for (a) unsupported α-$Ni(OH)_2$ and (b) supported α-$Ni(OH)_2$. The corresponding potentials at low and high current densities as a function of pH are depicted in (c) for the unsupported and (d) for the supported α-$Ni(OH)_2$.

Supported and unsupported α-$Ni(OH)_2$ display reaction orders with respect to hydroxyl of approximately 0 and ∼0.1, respectively. These values, while similar to one another, are distinctly different from what has been observed for carbon-supported MnO_x.[10] For carbon-supported MnO_x, the reaction order with respect to hydroxyl is −0.5, and for Ni-doped MnO_x the reaction order with respect to hydroxyl is −2. The reaction order with respect to hydroxyl for Pt_3Co is −0.5 and 0 for low and high current density regions, respectively.[36] The order of reaction with respect to hydroxyl concentration, and in general the sensitivity of the oxygen reduction reaction with respect to hydroxyl concentration, is typically interpreted to arise from two sources.[37] The first is that adsorbed hydroxyl may block active sites for O_2 adsorption. For most catalysts, higher solution concentration of hydroxyl results in a higher equilibrium surface concentration, and hence more site blocking. The observation that the chemical reaction rate constant increases as a function of OH^- concentration indicates that OH^- probably does not retard O_2 adsorption on the α-$Ni(OH)_2$ catalysts. The other mechanism by which hydroxyl is typically thought to steer the kinetics of the oxygen reduction reaction is by varying the binding energy of reaction intermediates. Again, it has been hypothesized that higher solution concentration of OH^- would result in higher surface coverage and more profound effect on intermediate binding energies. In the case of the present α-$Ni(OH)_2$ catalysts, since the order of reaction with respect to hydroxyl is 0 to 0.1, the catalyst displays diminished sensitivity to hydroxyl concentration. We propose that the tolerance of the α-$Ni(OH)_2$ catalysts to OH^- concentration arises because the catalyst surface is pre-hydroxylated. As such, sites for hydroxyl adsorption are already occupied on the catalyst surface, and the equilibrium concentration of hydroxyl on the surface may be decoupled from the solution phase hydroxyl concentration. Thus, variations in solution phase hydroxyl concentration would not diminish reaction rate.

Conclusions

The kinetics of the oxygen reduction reaction on α-$Ni(OH)_2$/GO and α-$Ni(OH)_2$ are studied using rotating disk linear sweep voltammetry at a range of oxygen and hydroxyl concentrations. Irrespective of the pH, the electron transfer number on the unsupported catalysts is 2.9 ± 0.2. On the GO supported catalyst the electron transfer number is 3.4 ± 0.1 at low hydroxyl concentration and 3.8–3.9 at $[OH^-] = 0.5M$. The electron transfer numbers indicate that while both supported and unsupported α-$Ni(OH)_2$ simultaneously catalyze the two and four electron pathways, the four electron pathway is relatively more dominant on the GO supported catalyst. Rotating ring disk studies are planned to further investigate the role intermediate desorption may play in the variation of electron transfer numbers.

In addition to having higher electron transfer numbers, the α-$Ni(OH)_2$/GO catalyst has a greater kinetic rate constant as compared to unsupported $Ni(OH)_2$. The higher kinetic rate constant is due to contributions from a higher chemical reaction rate constant and from a higher electron transfer rate constant. The higher chemical reaction rate constant may suggest a lower activation energy for adsorption of O_2 on the supported catalyst. Density functional theory calculations are underway to investigate the hypothesis that modification of the O_2 adsorption energy may contribute to the synergy between the α-$Ni(OH)_2$ catalyst and the GO support. Increased electron transfer rates may also contribute to the support/catalyst synergy as suggested by the higher electron transfer rate constant on the GO supported catalyst.

The order of reaction with respect to oxygen for both α-$Ni(OH)_2$/GO and α-$Ni(OH)_2$ is ∼1, similar to other transition metals and metal oxides. The orders of reaction with respect to hydroxyl for α-$Ni(OH)_2$/GO and α-$Ni(OH)_2$ are 0 and 0.1, respectively. These values are unusual as most of the transition metal and metal oxide catalysts display negative orders of reaction with respect to hydroxyl concentration. We hypothesize that the tolerance of the α-$Ni(OH)_2$/GO and α-$Ni(OH)_2$ catalysts to solution phase hydroxyl concentration arises because the surfaces of the α-$Ni(OH)_2$ catalysts are pre-hydroxylated. Hence, the equilibrium concentration of surface hydroxyl may not vary with solution concentration. Instead it is inherent to the catalyst structure. The tolerance of these α-$Ni(OH)_2$ catalysts to solution hydroxyl concentration suggests that they may be particularly useful for applications in which high hydroxyl concentrations are desired or in which the catalyst must operate stably under changing hydroxyl concentrations.

Acknowledgments

This research used resources of the Center for Functional Nanomaterials, which is a U.S. DOE Office of Science Facility, at Brookhaven National Laboratory under Contract No. DE-SC0012704. In addition, the authors gratefully acknowledge financial support of this work by the Air Force Research Labs under UES subcontract S-953-19-MR001. The authors thank the Advanced Imaging Facility of the College of Staten Island for SEM images, and Prof. William L'Amoreaux and Dr. Mike Bucaro for their help with SEM images.

References

1. J. S. Lee, S. T. Kim, R. Cao, N. S. Choi, M. Liu, K. T. Lee, and J. Cho, Metal-Air Batteries with High Energy Density: Li-Air versus Zn-Air. *Adv Energy Mater*, **1**(1), 34 (2011).
2. Y. S. Li, T. S. Zhao, and Z. X. Liang, Performance of alkaline electrolyte-membrane-based direct ethanol fuel cells. *J Power Sources*, **187**(2), 387 (2009).
3. I. Kruusenberg, L. Matisen, Q. Shah, A. M. Kannan, and K. Tammeveski, Non-platinum cathode catalysts for alkaline membrane fuel cells. *Int J Hydrogen Energ*, **37**(5), 4406 (2012).
4. X. G. Li, B. N. Popov, T. Kawahara, and H. Yanagi, Non-precious metal catalysts synthesized from precursors of carbon, nitrogen, and transition metal for oxygen reduction in alkaline fuel cells. *J Power Sources*, **196**(4), 1717 (2011).
5. N. Ramaswamy and S. Mukerjee, Influence of Inner- and Outer-Sphere Electron Transfer Mechanisms during Electrocatalysis of Oxygen Reduction in Alkaline Media. *J Phys Chem C*, **115**(36), 18015 (2011).
6. H. Q. Dong, Y. Y. Chen, M. Han, S. L. Li, J. Zhang, J. S. Li, Y. Q. Lan, Z. H. Dai, and J. C. Bao, Synergistic effect of mesoporous Mn2O3-supported Pd nanoparticle catalysts for electrocatalytic oxygen reduction reaction with enhanced performance in alkaline medium. *J Mater Chem A*, **2**(5), 1272 (2014).
7. M. Lefevre, E. Proietti, F. Jaouen, and J. P. Dodelet, Iron-Based Catalysts with Improved Oxygen Reduction Activity in Polymer Electrolyte Fuel Cells. *Science*, **324**(5923), 71 (2009).
8. F. H. B. Lima, M. L. Calegaro, and E. A. Ticianelli, Investigations of the catalytic properties of manganese oxides for the oxygen reduction reaction in alkaline media. *J Electroanal Chem*, **590**(2), 152 (2006).
9. Y. Y. Liang, Y. G. Li, H. L. Wang, J. G. Zhou, J. Wang, T. Regier, and H. J. Dai, Co_3O_4 nanocrystals on graphene as a synergistic catalyst for oxygen reduction reaction. *Nat Mater*, **10**(10), 780 (2011).
10. I. Roche, E. Chainet, M. Chatenet, and J. Vondrak, Carbon-supported manganese oxide nanoparticles as electrocatalysts for the Oxygen Reduction Reaction (ORR) in alkaline medium: Physical characterizations and ORR mechanism. *J Phys Chem C*, **111**(3), 1434 (2007).
11. Y. Wang, D. Zhang, and H. Q. Liu, A study of the catalysis of cobalt hydroxide toward the oxygen reduction in alkaline media. *J Power Sources*, **195**(10), 3135 (2010).
12. Q. M. Wu, L. H. Jiang, Q. W. Tang, J. Liu, S. L. Wang, and G. Q. Sun, Activity and stability of the Ni(OH)(2)-MnOx/C composite for oxygen reduction reaction in alkaline solution. *Electrochim Acta*, **91**, 314 (2013).
13. E. Farjami, M. A. Rottmayer, and L. J. Deiner, Evidence for oxygen reduction reaction activity of a Ni(OH)(2)/graphene oxide catalyst. *J Mater Chem A*, **1**(48), 15501 (2013).
14. Z. X. Liu, Z. P. Li, H. Y. Qin, and B. H. Liu, Oxygen reduction reaction via the 4-electron transfer pathway on transition metal hydroxides. *J Power Sources*, **196**(11), 4972 (2011).
15. C. Song and J. Zhang, *PEM Fuel Cell Electrocatalysts and Catalyst Layers*. 1 ed.; Springer-Verlag London: 2008.
16. J. T. Zhang, C. X. Guo, L. Y. Zhang, and C. M. Li, Direct growth of flower-like manganese oxide on reduced graphene oxide toward efficient oxygen reduction reaction. *Chem Commun*, **49**(56), 6334 (2013).
17. W. Xiao, D. L. Wang, and X. W. Lou, Shape-Controlled Synthesis of MnO_2 Nanostructures with Enhanced Electrocatalytic Activity for Oxygen Reduction. *J Phys Chem C*, **114**(3), 1694 (2010).
18. M. Chatenet, L. Genies-Bultel, M. Aurousseau, R. Durand, and F. Andolfatto, Oxygen reduction on silver catalysts in solutions containing various concentrations of sodium hydroxide - comparison with platinum. *J Appl Electrochem*, **32**(10), 1131 (2002).
19. L. Genies, Y. Bultel, R. Faure, and R. Durand, Impedance study of the oxygen reduction reaction on platinum nanoparticles in alkaline media. *Electrochim Acta*, **48**(25-26), 3879 (2003).
20. L. Genies, R. Faure, and R. Durand, Electrochemical reduction of oxygen on platinum nanoparticles in alkaline media. *Electrochim Acta*, **44**(8-9), 1317 (1998).
21. T. S. Light, Standard Solution for Redox Potential Measurements. *Anal Chem*, **44**(6), 1038–& (1972).
22. A. J. Bard and L. R. Faulkner, *Electrochemical Methods: Fundamentals and Applications*. 2 ed.; John Wiley & Sons, Inc: 2001.
23. R. Z. Jiang and F. C. Anson, The Origin of Inclined Plateau Currents in Steady-State Voltammograms for Electrode Processes Involving Electrocatalysis. *J Electroanal Chem*, **305**(2), 171 (1991).
24. A. Sarapuu, K. Tammeveski, T. T. Tenno, V. Sammelselg, K. Kontturi, and D. J. Schiffrin, Electrochemical reduction of oxygen on thin-film. Au electrodes in acid solution. *Electrochem Commun*, **3**(8), 446 (2001).
25. N. A. Savastenko, K. Anklam, A. Quade, M. Bruser, A. Schmuhl, and V. Bruser, Comparative study of plasma-treated non-precious catalysts for oxygen and hydrogen peroxide reduction reactions. *Energ Environ Sci*, **4**(9), 3461 (2011).
26. M. S. El-Deab and T. Ohsaka, Hydrodynamic voltammetric studies of the oxygen reduction at gold nanoparticles-electrodeposited gold electrodes. *Electrochim Acta*, **47**(26), 4255 (2002).
27. B. Huskinson, M. P. Marshak, C. Suh, S. Er, M. R. Gerhardt, C. J. Galvin, X. D. Chen, A. Aspuru-Guzik, R. G. Gordon, and M. J. Aziz, A metal-free organic-inorganic aqueous flow battery. *Nature*, **505**(7482), 195–+ (2014).
28. D. Zhang, D. H. Chi, T. Okajima, and T. Ohsaka, Catalytic activity of dual catalysts system based on nano-manganese oxide and cobalt octacyanophthalocyanine toward four-electron reduction of oxygen in alkaline media. *Electrochim Acta*, **52**(17), 5400 (2007).
29. R. E. Davis, G. L. Horvath, and C. W. Tobias, The solubility and diffusion coefficient of oxygen in potassium hydroxide solutions. *Electrochim Acta*, **12**, 287 (1967).
30. E. Narita, F. Lawson, and K. N. Han, Solubility of Oxygen in Aqueous-Electrolyte Solutions. *Hydrometallurgy*, **10**(1), 21 (1983).
31. D. Tromans, Modeling oxygen solubility in water and electrolyte solutions. *Ind Eng Chem Res*, **39**(3), 805 (2000).
32. H. Meng and P. K. Shen, Novel Pt-free catalyst for oxygen electroreduction. *Electrochem Commun*, **8**(4), 588 (2006).
33. X. X. Li, A. L. Zhu, W. Qu, H. J. Wang, R. Hui, L. Zhang, and J. J. Zhang, Magneli phase Ti_4O_7 electrode for oxygen reduction reaction and its implication for zinc-air rechargeable batteries. *Electrochim Acta*, **55**(20), 5891 (2010).
34. E. Yeager, Dioxygen electrocatalysis: mechanism in relation to catalyst structure. *J Mol Catal*, **38**, 5 (1986).
35. C. C. Chang, T. C. Wen, and H. J. Tien, Kinetics of oxygen reduction at oxide-derived Pd electrodes in alkaline solution. *Electrochim Acta*, **42**(4), 557 (1997).
36. M. D. Obradovic, B. N. Grgur, and L. M Vracar., Adsorption of oxygen containing species and their effect on oxygen reduction on Pt3Co electrode. *J Electroanal Chem*, **548**, 69 (2003).
37. T. J. Schmidt, V. Stamenkovic, P. N. Ross, and N. M. Markovic, Temperature dependent surface electrochemistry on Pt single crystals in alkaline electrolyte - Part 3. The oxygen reduction reaction. *Phys Chem Chem Phys*, **5**(2), 400 (2003).
38. W. M. Haynes, *CRC Handbook of Chemistry and Physics*. 95th ed.; 2014.